Seismic reliability-based design of hardening structures equipped with double sliding devices

COMPDYN 2019
7th ECCOMAS Thematic Conference on
Computational Methods in Structural Dynamics and Earthquake Engineering
M. Papadrakakis, M. Fragiadakis (eds.)
Crete, Greece, 24–26 June 2019

SEISMIC RELIABILITY-BASED DESIGN OF HARDENING STRUCTURES EQUIPPED WITH DOUBLE SLIDING DEVICES

Paolo Castaldo[1], Gaetano Alfano[2], Diego Gino[3], Costanza Anerdi[4] and Giuseppe Carlo Marano[5]

[1] Department of Structural, Geotechnical and Building Engineering (DISEG), Politecnico di Torino, Turin, Italy
corso Duca degli Abuzzi 24, 10129 Torino, ITALY
e-mail: paolo.castaldo@polito.it

[2] Department of Structural, Geotechnical and Building Engineering (DISEG), Politecnico di Torino, Turin, Italy
corso Duca degli Abuzzi 24, 10129 Torino, ITALY
e-mail: gae.alfano@gmail.com

[3] Department of Structural, Geotechnical and Building Engineering (DISEG), Politecnico di Torino, Turin, Italy
corso Duca degli Abuzzi 24, 10129 Torino, ITALY
e-mail: diego.gino@polito.it

[4] Department of Structural, Geotechnical and Building Engineering (DISEG), Politecnico di Torino, Turin, Italy
corso Duca degli Abuzzi 24, 10129 Torino, ITALY
e-mail: costanza.anerdi@polito.it

[5] Department of Structural, Geotechnical and Building Engineering (DISEG), Politecnico di Torino, Turin, Italy
corso Duca degli Abuzzi 24, 10129 Torino, ITALY
e-mail: giuseppe.marano@polito.it

Abstract

This study deals with seismic reliability-based design (SRBD) relationships in terms of behavior factors and displacement demands for hardening structures equipped with double friction pendulum system (DFPS) bearings. An equivalent 3dof system having a hardening post-yield slope is adopted to describe the superstructure behavior, whereas velocity-dependent laws are assumed to model the responses of the two surfaces of the DFPS. The yielding characteristics of the superstructures are defined for increasing behavior factors in compliance with the seismic hazard of L'Aquila site (Italy) and with NTC18 assuming a lifetime of 50 years. Considering several natural seismic records and building properties under the hypothesis of modelling the friction coefficients of the two surfaces of the DFPS as random va-

riables, incremental dynamic analyses are performed to evaluate the seismic fragility and the seismic reliability of these systems. Finally, seismic reliability is evaluated and seismic reliability-based design (SRBD) curves for the two surfaces of the double sliding devices are described.

Keywords: behavior factor, ductility demand, friction pendulum bearing, post-yield hardening stiffness, seismic isolation, seismic reliability.

1 INTRODUCTION

A very effective technique for the seismic isolation[1] of building frames and infrastructure is represented by the sliding pendulum bearings [2]-[3] examined by several literature studies (e.g., [4]-[7]). Probabilistic analyses and reliability-based analyses have also been presented by [8]-[9] as well as reliability analysis and reliability-based optimization of base-isolated systems including the main uncertainties have been performed by [10]-[14]. A non-dimensionalization of the motion equations governing the dynamic response of equivalent two-degree-of-freedom (2dof) models equipped with friction pendulum system (FPS) isolators has been proposed by [15]. In the hypothesis that the friction coefficient and the earthquake main characteristics are the relevant random variables, seismic reliability analyses of a 3D base-isolated r.c. system have been developed in Castaldo et al. [16] and Palazzo et al. [17] to propose a method useful to design the isolator dimensions in plan. The life-cycle cost analysis (LCCA) of a r.c. 3D structure isolated by FPS bearings has been examined by [18] to evaluate the dependence on increasing isolation degrees. The approach for a seismic reliability-based design (SRBD) of elastic systems isolated by FPS has been generalized in Castaldo et al. [19] for a wide range of structural properties. A robustness analysis in reliability terms of a r.c. 3D building frame isolated by FPS devices in presented in [20] proposing the failure scenarios if a malfunction affects a seismic device together with the design solution. The literature studies of [21] and [22] proposed, respectively, the optimal values of the friction coefficient, on the one hand, as a function of the system properties and of the soil condition in order to minimize the superstructure response and, on the other, as a function of the ground motion characteristics by means of the ratio PGA/PGV (peak ground acceleration/velocity). In [23], a robust design optimization (RDO) of base isolation system considering random system parameters characterizing the structure, isolator and ground motion model, is performed by minimizing the weighted sum of the expected value of the maximum root mean square acceleration of the structure as well its standard deviation. In [24], an optimal design of frictional devices is proposed by applying a Pareto-type optimization approach.

The seismic performance of bridges or structures isolated with FPS or DFPS has been investigated in [25]-[31]. Specifically, [28]-[30]provide useful relationships, according also to experimental results, for the evaluation of the seismic response of structures isolated by DFPS together with the equations governing the dynamic behaviour of these devices. The principal benefit of the DFPS bearing is its capacity to accommodate substantially larger displacements compared to a traditional FP bearing of identical plan dimensions as discussed in [28]. In [26] and [31], the seismic performance of isolated bridge and liquid storage tanks are respectively investigated, considering different combinations of radii of curvature and friction coefficients.

As for the design of base-isolated systems under strong earthquake events, seismic code provisions [32]-[36] are based on low values of the strength reduction factor [32]-[36] or behavior factor [33]-[34] to ensure a safety level against the non linear dynamic amplification phenomenon (partial resonance) [37]. Precisely, NTC18 [34], Eurocode 8 [33] and the Japanese building code [35] provide a maximum behavior factor value of 1.5, without explicitly distinguishing between the ductility and overstrength factor terms, ASCE 7 [32] prescribes a value equal to 0.375 times the one for corresponding fixed-base systems and no larger than 2. In this context, Vassiliou et al. [38] obtained that the displacement ductility demand of the inelastic base-isolated structure is 3 times the strength reduction factor confirming that, for base-isolated structures, it is not possible to adopt the formulas relating the strength reduction factor R and the displacement ductility demand μ of Newmark and Hall [39] and of Miranda and Bertero [40]. Then, seismic reliability-based relationships between the ductility-dependent strength reduction factors and the displacement ductility demand, respectively, for

equivalent perfectly elastoplastic and hardening structural systems equipped with FPS depending on the structural properties have been proposed in [41],[42].

Inspired by [41],[42], this study proposes reliability-based design regressions relating the behavior factors and the displacement ductility demands for hardening structural systems equipped with double friction pendulum system (DFPS) devices and considering a high seismic hazard site like L'Aquila (Italy). By means of an equivalent 3dof system, different elastic and inelastic structural system properties are investigated. Specifically, the yielding characteristics of the hardening superstructures are designed in compliance with the life safety limit state and with the seismic hazard of L'Aquila site (Italy) assuming a lifetime of 50 years and increasing behavior factors [32]-[35]. The model developed by [4] is used to describe the non-linear velocity-dependent behavior of the two surfaces of the DFPS. The study is also based on the hypothesis of assuming the both friction coefficients of the two surfaces of the DFPS and the characteristics of the records as the relevant random variables. In detail, appropriate Gaussian probability density functions (PDFs) are adopted to characterize the aleatory uncertainties of the both sliding friction coefficients and, by means of the Latin Hypercube Sampling (LHS) method [43]-[45], the input data have been generated.

Then, several incremental dynamic analyses (IDAs) are performed for increasing seismic intensity levels in compliance with the site seismic hazard to derive the seismic fragility curves related to the different degrees of freedom of the equivalent (3dof) system. Finally, by means of the convolution integral between the fragility curves and the seismic hazard curves of L'Aquila site (Italy), in the hypothesis of a design life of 50 years for the equivalent base-isolated systems, the corresponding reliability curves are derived.

2 EQUATIONS OF MOTION FOR NON-LINEAR HARDENING STRUCTURAL SYSTEMS WITH DOUBLE CONCAVE SLIDING BEARINGS

The equivalent model, herein employed and depicted in Fig. 1, is a 3dof system with a dof representative of the superstructure behaviour and two dofs representative of the responses of the two surfaces of the DFPS. The model takes into account the inelastic hardening response of the superstructure and non-linear behaviours of the two surfaces of the DFPS [28].

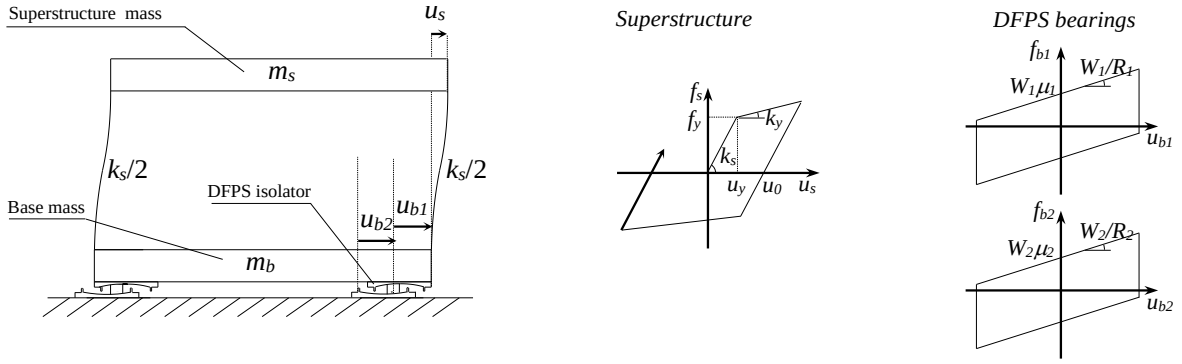

Figure 1: 3dof model of an inelastic hardening building frame isolated with DFPS.

Regarding the free body diagram of the DFPS, the bearing restoring force, considering only the horizontal component of the displacement on each surface, is:

$$f_{b,1} = \frac{W_1}{R_1} u_{b,1} + \mu_{d,1} W_1 \operatorname{sgn}\left(\dot{u}_{b,1}\right)$$
$$f_{b,2} = \frac{W_2}{R_2} u_{b,2} + \mu_{d,2} W_2 \operatorname{sgn}\left(\dot{u}_{b,2}\right) \quad (1)$$

where $W_1 = (m_b + m_s)g$ is the weight on the upper surface (surface 1) of the bearing, $W_2 = (m_b + m_s + m_d)g$ is the weight on the lower surface (surface 2) of the bearing, g is the gravity constant, R_1 and R_2 are the radii of curvature of the two surfaces of the device, $u_{b,1}$ denotes the displacement of the surface 1 with respect to the slider, $u_{b,2}$ represents the slider displacement with respect to the ground as well as $\mu_{d,1}$ and $\mu_{d,2}$ are the sliding friction coefficients of the two surfaces and sgn is the signum function of the sliding velocity for each surface. In this study, the upper surface (surface 1) is characterized by higher values of the friction coefficient and of the radius of curvature. Specifically, $\mu_{d,1}$ is selected as $4\mu_{d,2}$ and $R_1=2R_2$ [28]-[31]. The force of the bearing coincides with the force of each surface response $f_b = f_{b,1} = f_{b,2}$. For each surface, the friction coefficient is given as a function of the sliding velocity [4]-[6]:

$$\mu_{d,i} = f_{\max,i} - \left(f_{\max,i} - f_{\min,i}\right)\exp\left(-\alpha \dot{u}_{b,i}\right) \quad \text{for } i = 1,2 \tag{2}$$

where $f_{\max,i}$ and $f_{\min,i}$ are, respectively, the friction coefficients at high and very low sliding velocities of the i-th surface, α is a constant set equal to 30 as well as the ratio $f_{\max,i} / f_{\min,i}$ equal to 3 for each surface [15]-[21],[41].

A bilinear constitutive law describes the inelastic hardening behaviour of the superstructure, which responses in elastic phase if Eqn.(3) is satisfied and the restoring force $f_{s,i}$ is expressed by Eqn.(4):

$$\left|u_{s,i} - u_{0,i-1}\right| < y\left(u_{s,i}\right) \tag{3}$$

$$f_{s,i}\left(u_{s,i}\right) = k_s\left(u_{s,i} - u_{0,i-1}\right) \tag{4}$$

where $f_{s,i}$ is the restoring force at time instant i, $u_{s,i}$ is the superstructure deformation at the same instant, $u_{0,i-1}$ is the maximum plastic excursion at time instant $(i-1)$ and k_s is the elastic stiffness of the superstructure. The function $y(u_{s,i})$ is the yielding condition in function of the displacement and is non-univocally defined due to the translation of the elastic domain [46]. Defining u_y as the yield displacement, whose yield force is f_y, H denotes the ratio between the hardening post-yield and the elastic stiffness [47]-[48], evaluated as:

$$H = S = \frac{k_y}{k_s} \tag{5}$$

The superstructure response is plastic if Eqn.(6) is satisfied and the restoring force applies according to Eqn.(7):

$$\left|u_{s,i} - u_{0,i-1}\right| \geq y(u_{s,i}) \tag{6}$$

$$f_{s,i}\left(u_s\right) = k_s(u_{s,i} - y(u_{s,i}))\,\mathrm{sgn}(u_{s,i} - u_{0,i-1}) \tag{7}$$

Therefore, the equations which describe the response of an inelastic 3dof system, isolated by DFPS devices, to the seismic input $\ddot{u}_g(t)$, without any viscous property for the DFPS, are:

$$
\begin{aligned}
&m_s\ddot{u}_s + (m_s + m_b)\ddot{u}_{b,1} + (m_s + m_b + m_d)\ddot{u}_{b,2} + \frac{W_2}{R_2}u_{b,2} + W_2\mu_2\,\mathrm{sgn}\left(\dot{u}_{b,2}\right) = -(m_s + m_b + m_d)\ddot{u}_g \\
&m_s\ddot{u}_s + (m_s + m_b)\ddot{u}_{b,1} + (m_s + m_b)\ddot{u}_{b,2} + (m_s + m_b)\frac{g}{R_1}u_{b,1} + (m_s + m_b)g\mu_1\,\mathrm{sgn}\left(\dot{u}_{b,1}\right) = -(m_s + m_b)\ddot{u}_g \\
&m_s\ddot{u}_s + m_s\ddot{u}_{b,1} + m_s\ddot{u}_{b,2} + c_s\dot{u}_s + f_{s,i}(u_s) = -m_s\ddot{u}_g
\end{aligned}
\tag{8}
$$

where m_s, m_b and m_d are respectively the mass of the superstructure, of the isolation level and of the slider, c_s is the viscous damping factor of the superstructure. Dividing Eqn.(8a) by $m_s + m_b + m_d$ as well as Eqn.(8b) by $m_b + m_s$ and Eqn.(8c) by m_s, defining the mass ratios as $\gamma_s = m_s/(m_s + m_b + m_d)$, $\gamma_b = m_b/(m_s + m_b + m_d)$ and $\gamma_d = m_d/(m_s + m_b + m_d)$ [49], the isolation $\omega_{b,i} = \sqrt{g/R_i}$ and structural $\omega_s = \sqrt{k_s/m_s}$ circular frequency, the structural damping ratio $\xi_s = c_s/2m_s\omega_s$, the non-dimensional equations apply:

$$
\begin{aligned}
&\gamma_s\ddot{u}_s + (\gamma_s + \gamma_b)\ddot{u}_{b,1} + \ddot{u}_{b,2} + \omega_{b,2}^2 u_{b,2} + g\mu_2\,\mathrm{sgn}\left(\dot{u}_{b,2}\right) = -\ddot{u}_g \\
&\gamma_s\ddot{u}_s + (\gamma_s + \gamma_b)\ddot{u}_{b,1} + (\gamma_s + \gamma_b)\ddot{u}_{b,2} + (\gamma_s + \gamma_b)\omega_{b,1}^2 u_{b,1} + (\gamma_s + \gamma_b)g\mu_1\,\mathrm{sgn}\left(\dot{u}_{b,1}\right) = -(\gamma_s + \gamma_b)\ddot{u}_g \\
&\ddot{u}_s + \ddot{u}_{b,1} + \ddot{u}_{b,2} + 2\omega_s\xi_s\dot{u}_s + a_s(u_s) = -\ddot{u}_g
\end{aligned}
\tag{9}
$$

where $a_s\left(u_s\right) = f_s\left(u_s\right)/m_s$ is the dimensionless force of the superstructure that depends, respectively, on the stiffness k_s in the elastic phase and on the yielding condition in the plastic phase. Note that the elastic isolation period of vibration varies if the sliding movement occurs along surface 1 or surface 2 or along the both surfaces simultaneously [30]. Specifically, if the sliding movement is developed along only a surface, the isolation period depends only on the radius of curvature of the spherical surface R_i (i.e., typically the radius of the surface with the lower friction coefficient) and the bearing behaves like a simple FPS [19], whereas when the both surfaces are involved, the isolation effective period applies [30]:

$$
T_b = 2\pi\sqrt{\frac{R_1 + R_2}{g}} \tag{10}
$$

The change of the vibration period shows the adaptive behavior to the seismic intensity that characterizes these devices [28]-[30]. It follows that the ratio between the variable isolation period and structural period of vibration, which defines the seismic isolation degree [52] cannot be a constant during an earthquake event. Moreover, when the both surfaces slide simultaneously the restoring force of the DFPS device can be evaluated as $\mu_e W_1$ neglecting the mass of the slider [28], where μ_e is the effective sliding coefficient given by:

$$
\mu_e = \frac{\mu_{d,1}R_1 + \mu_{d,2}R_2}{R_1 + R_2} \tag{11}
$$

2.1 Inelastic properties of the superstructure

The inelastic behavior of the superstructure is assumed as an equivalent sdof system [50]-[51] having a hardening post-yield stiffness. The behavior factor, *q*, and displacement ductility, μ , are defined, respectively, as:

$$
q = \frac{f_{s,el}}{f_y} = \frac{u_{s,el}}{u_y} \tag{12}
$$

$$\mu = \frac{u_{\mathrm{s,max}}}{u_y} \tag{13}$$

where $f_{s,el}$ and $u_{s,el}$ are, respectively, the peak elastic response values required to the superstructure, whereas $u_{\mathrm{s,max}} = \left|u_s(t)\right|_{\max}$ is the peak inelastic displacement during a ground motion. This behaviour factor *q* is consistent with the codes [32]-[36] and with the study [42].

3 UNCERTAINTIES RELEVANT TO THE PERFORMANCE ASSESSMENT

For the seismic reliability assessment of a building frame, within the structural performance (SP) evaluation method [53]-[55], specific correlations between the SP levels [56] and appropriate exceeding probabilities during its design life [57]-[58] as well as the relevant (aleatory and/or epistemic) uncertainties with the corresponding PDFs have to be defined. According to the PEER-like modular approach [59] and performance-based earthquake engineering (PBEE) approach [60]-[61], distinguishing the aleatory uncertainties related to the seismic input intensity from those corresponding to the characteristics of the record by means of an intensity measure (IM), this work evaluates and quantifies the seismic reliability of hardening systems equipped with DFPS, located in L'Aquila site (Italy), assuming also the friction coefficients as other relevant random variables. Other aleatory uncertainties are not modelled since their effects can be neglected as discussed in [41],[62]. The epistemic uncertainties are not considered in this study. Specifically, a Gaussian PDF truncated on both sides to 2% and 6% with a mean equal to 4% for the upper surface ($\mu_{d,1}$) and a Gaussian PDF truncated on both sides to 0.5% and 1.5% with a mean of 1% for the lower surface ($\mu_{d,2}$) are used to model, respectively, the sliding friction coefficients at large velocities of the two surfaces of the DFPS bearings [41]-[42]. These values are in compliance with [28]-[31] and chosen in order to obtain a mean value of the effective friction coefficient equal to 3% and, so to allow a comparison with the FPS analysed in [41]-[42]. Then, using the LHS technique [43]-[45], 15 sampled couples of the friction coefficients at large velocities are defined.

As for the uncertainty on the characteristics of the seismic records (record to record variability), according to PBEE approach [60]-[61] and similarly to [41]-[42], the spectral displacement $S_D(\xi_b, T_b)$, related to the equivalent effective period $T_b = 2\pi/\omega_b$ (Eq.(10)) and to damping ratio ξ_b [19],[41] is chosen as *IM* [64]-[66]. Considering ξ_b equal to zero [15],[41],[67], the corresponding IM is hereinafter denoted as $S_D(T_b)$ in the range from 0 m to 0.45 m according to the seismic hazard of L'Aquila site (Italy) [34]. The record-to-record variability is taken into account by means of 30 ground motion records, corresponding to 19 different earthquake events, selected form different national and international databases. A detailed description may be found in [41].

4 INCREMENTAL DINAMIC ANALYSES: RESULTS AND COMPARISON

The performance of hardening systems isolated with DFPS is evaluated through incremental dynamic analyses (IDAs), considering several structural parameters combination and L'Aquila (Italy) as the reference site.

4.1 Design of the elastic and inelastic properties of the structural systems

An extended parametric analysis is carried out considering the following deterministic parameters: isolation degree I_d, varying between 2, 4, 6 and 8 with respect to the equivalent

effective isolated period; the equivalent effective isolation period T_b , varying between 3s, 4s, 5s and 6s; the mass ratio γ_s, assumed equal to 0.6 and 0.8 with γ_d equal to 0.001 and so γ_b equal to 0.399 and 0.199; the behaviour factor q, ranging from 1.1 to 2, with a step of 0.1, according to the codes [32]-[35], and the post-yield hardening stiffness ratio *H*, set equal to 0.03 [47]-[51]. It follows that 384 equivalent 3dof systems, with isolation damping ratio ξ_b and superstructure damping ratio ξ_s respectively equal to 0% and 2%, are properly defined. These abovementioned 384 equivalent 3dof systems derive from 32 different 3dof systems (with the different values of I_d, of T_b and of the mass ratio) by modifying the behavior factor In the hypothesis of $\mu_{d,1}$ and $\mu_{d,2}$ equal to 4% and 1%, respectively, and a ratio equal to 2 between R_1 and R_2 [28]-[31], the yielding characteristics of 32 3dof elastic systems, necessary to perform IDAs, are evaluated considering the average elastic responses to the 30 seismic inputs scaled to the *IM* value of the life safety limit state for L'Aquila site (Italy): the $IM = S_D(T_b)$ applies 0.311 m for T_b=3, 4, 5 s and 0.26 m for T_b =6 s (NTC18 [34]). In this way, the average values in terms of both yield strength $f_{y,\text{average}}$ and displacement $u_{y,\text{average}}$ of the superstructure have been computed in Matlab-Simulink [72] and, the yielding properties are finally defined for each value of *q*, according to Eqn.(14):

$$u_{y,average} = \frac{f_{y,average}}{k_s} = \frac{f_{s,el,average}}{k_s q} = \frac{u_{s,el,average}}{q} \tag{14}$$

4.2 Incremental dynamic analysis (IDA) curves

This section describes the responses of the 384 equivalent 3dof hardening systems having different properties (i.e., I_d, T_b , γ_s, q, *H*) combined with the 15 sampled couples of the friction coefficients, to the 30 seismic inputs scaled to the different $IM = S_D(T_b)$, ranging from 0 m to 0.45 m. A total number of 450 numerical analyses has been performed for each *IM* level and parameter combination. The isolated non-linear hardening systems are modelled in Matlab-Simulink [72], by employing the Runge-Kutta-Fehlberg integration algorithm to solve the coupled equations (Eqn.(9)) and determine the responses of each degree of freedom. The results of the non-linear IDAs have made it possible to estimate the collapsed system cases as well as the superstructure and isolation response parameters, expressed, respectively, in terms of displacement ductility demand μ and of displacements for the DFPS (i.e., peak value for each surface or peak value of their sum computed at each time instant). These response parameters are assumed as the engineering demand parameters (EDPs) and their peak values have been fitted with lognormal distribution [15],[16]-[21],[41],[60],[67], by estimating the sample lognormal mean, $\mu_{\ln}(EDP)$, and the sample lognormal standard deviation $\sigma_{\ln}(EDP)$, or dispersion $\beta(EDP)$, through the maximum likelihood estimation technique, to determine the 50th, 84th and 16th percentile of each lognormal PDF [15]. Note that other uncertainties as well as aftershock events [73]-[83] and the contribution provided by the infills [84]-[89] are not considered in this study.

Figures 2-7 show the IDA results results corresponding to some parameters (I_d =2 and 8, T_b =3s and 6s and mainly related to γ_s equal to 0.6).

Fig.s 2-3 show the IDA results regarding the isolation level EDP $u_{b,\max}$, which is the peak value of the sum of $u_{b,1}$ and $u_{b,2}$ in each time instant, in the case of hardening structures. This

response parameter is important to design the elements and components at the isolation level and to estimate the maximum displacement of the isolation system. Therefore, the displacement $u_{b,\max}$ shown in Fig.s 2-3 is the maximum displacement recorded during the non-linear dynamic analysis, and generally is not concomitant with the maximum displacement recorded at each single surface. The lognormal mean of the EDP $u_{b,\max}$ increases by increasing T_b and I_d. Both the statistical values are also influenced by γ_s because the isolation displacement increases for lower values of γ_s. Moreover, the decrease of q has a slight effect on the isolation response leading to a slight increase of $u_{b,\max}$, especially for higher values of I_d. The results are roughly in accord with the ones obtained in [42] considering a single surface FPS.

Fig.s 4-5 show, respectively, the response in terms of the peak displacement of each surface of the DFPS: the displacement of the upper surface are higher than the displacement of the surface 2, characterized by a lower value of the radius of curvature.

Fig.s 6-7 show the IDA curves regarding the hardening superstructure EDP μ. The statistical parameters of the EDP μ highly depend on q because an its increase leads to a very high displacement ductility demand μ. In addition, the statistical value $\mu_{\ln}(\mu)$ highly increases by increasing T_b but decreases for higher values of I_d, especially for high values of T_b. Moreover, with reference to the effects of γ_s on the both superstructure statistics, the increase of mass ratio leads to an increase of the superstructure response.

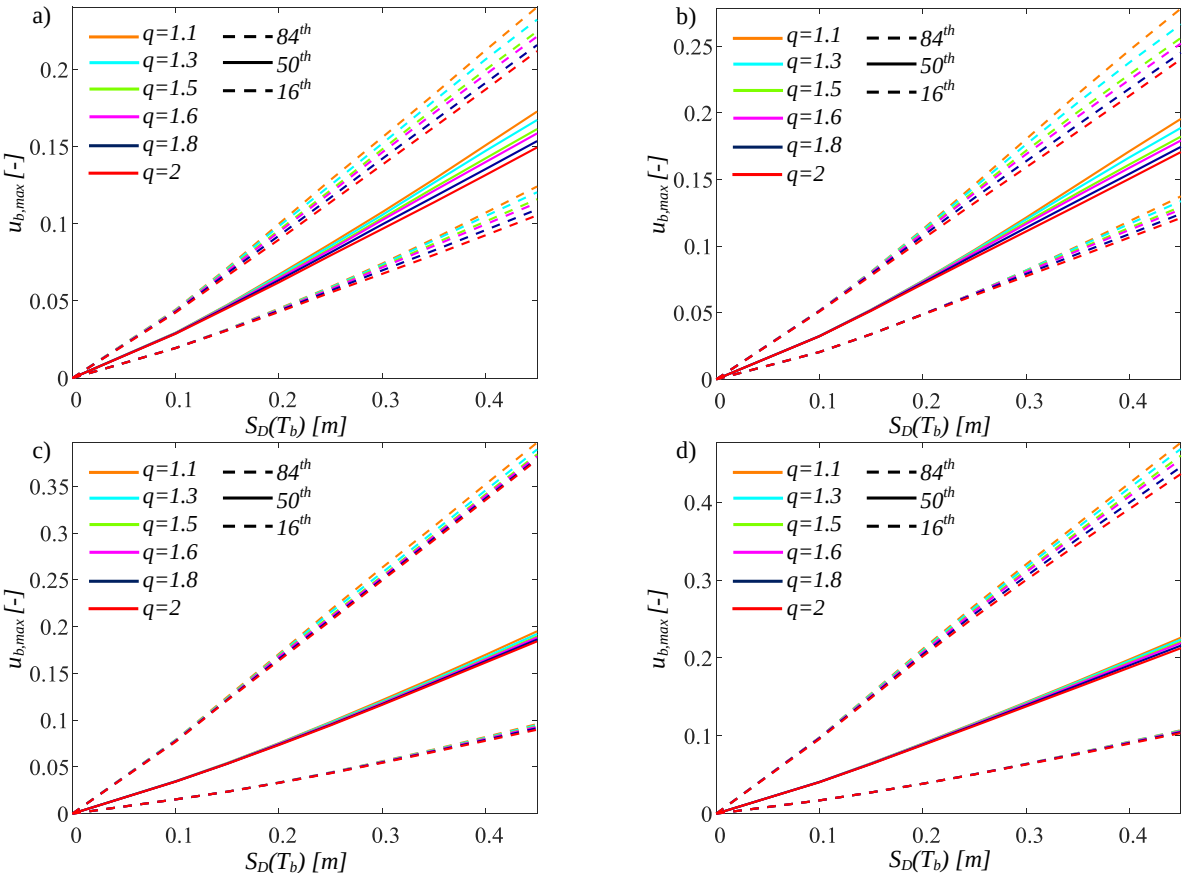

Figure 2: IDA curves of the isolation level with γ_s=0.6 for I_d=2, T_b=3 s, H=0.03 (a), I_d=2, T_b=6 s, H=0.03 (b), I_d=8, T_b=3 s, H=0.03 (c), I_d=8, T_b=6 s, H=0.03 (d).

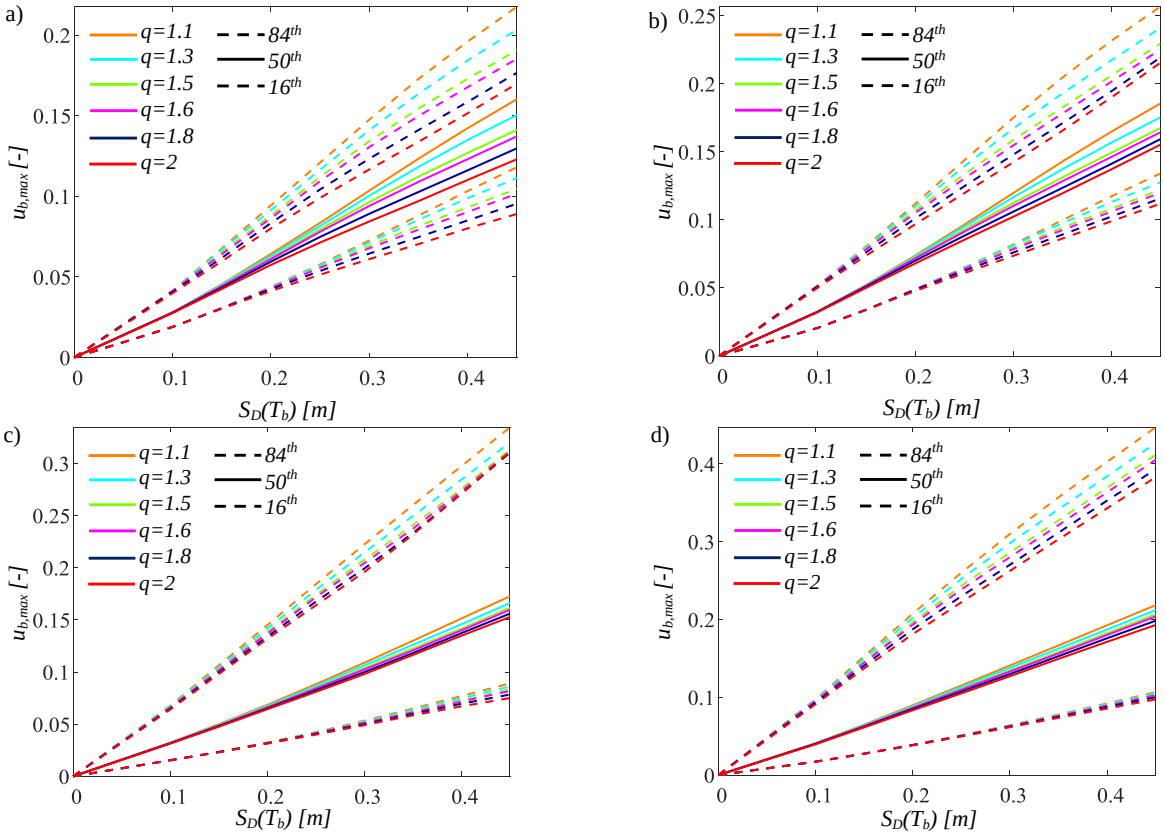

Figure 3: IDA curves of the isolation level with γ_s=0.8 for I_d=2, T_b=3 *s*, H=0.03 (a), I_d=2, T_b=6 s, H=0.03 (b), I_d=8, T_b=3 s, H=0.03 (c), I_d=8, T_b=6 s, H=0.03 (d).

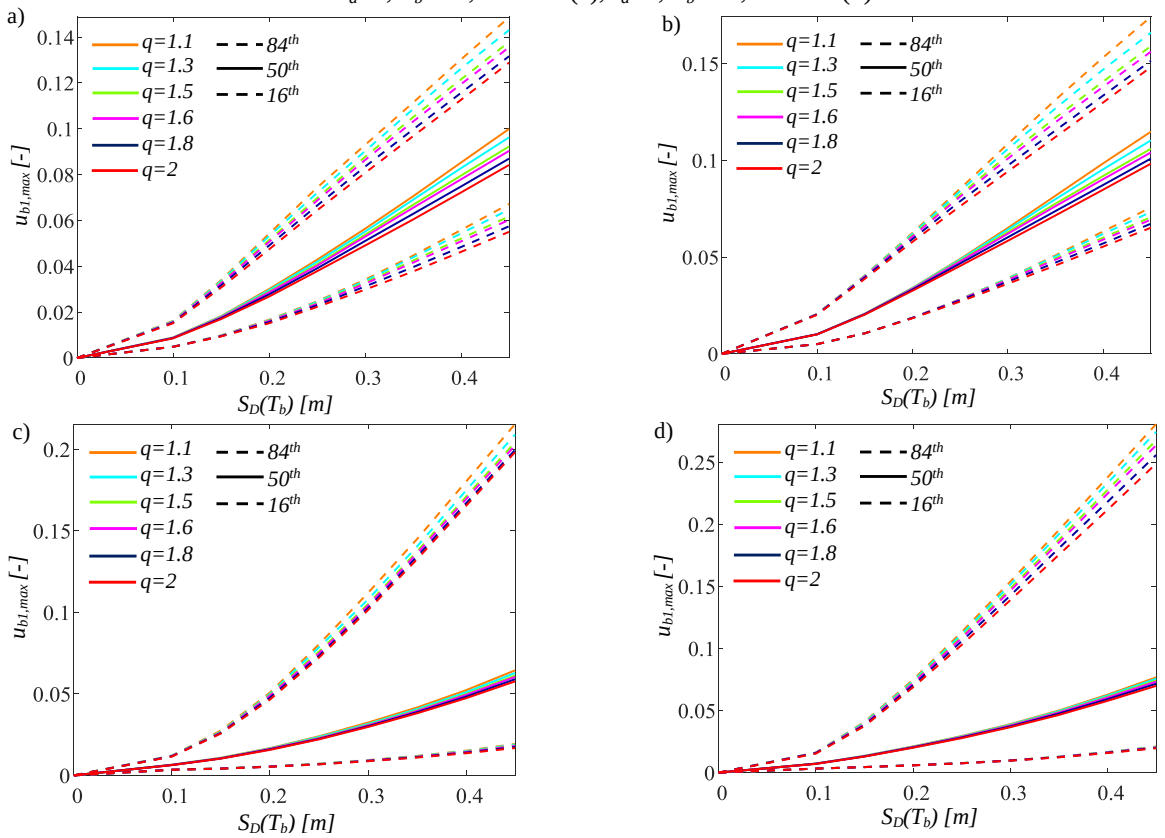

Figure 4: IDA curves of the sliding surface 1 with γ_s=0.6 for I_d=2, T_b=3 *s*, H=0.03 (a), I_d=2, T_b=6 s, H=0.03 (b), I_d=8, T_b=3 s, H=0.03 (c), I_d=8, T_b=6 s, H=0.03 (d).

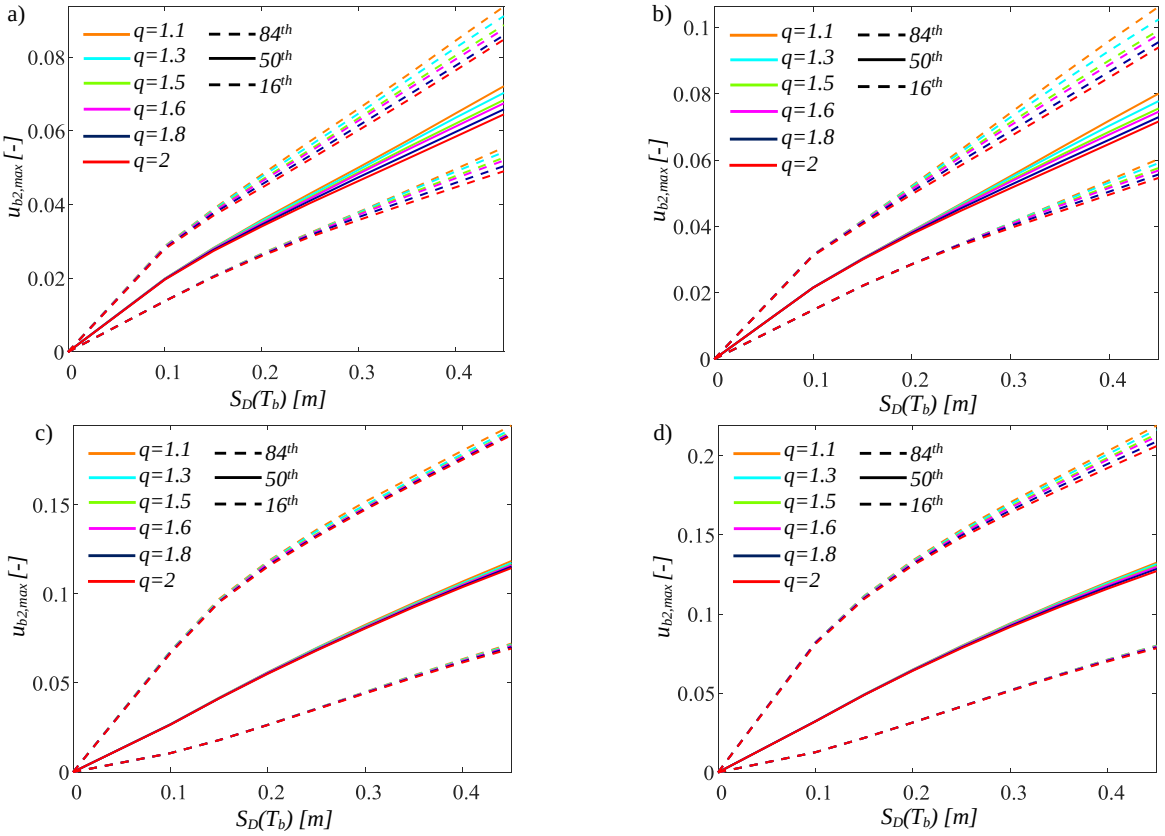

Figure 5: IDA curves of the sliding surface 2 with γ_s=0.6 for I_d=2, T_b=3 s, H=0.03 (a), I_d=2, T_b=6 s, H=0.03 (b), I_d=8, T_b=3 s, H=0.03 (c), I_d=8, T_b=6 s, H=0.03 (d).

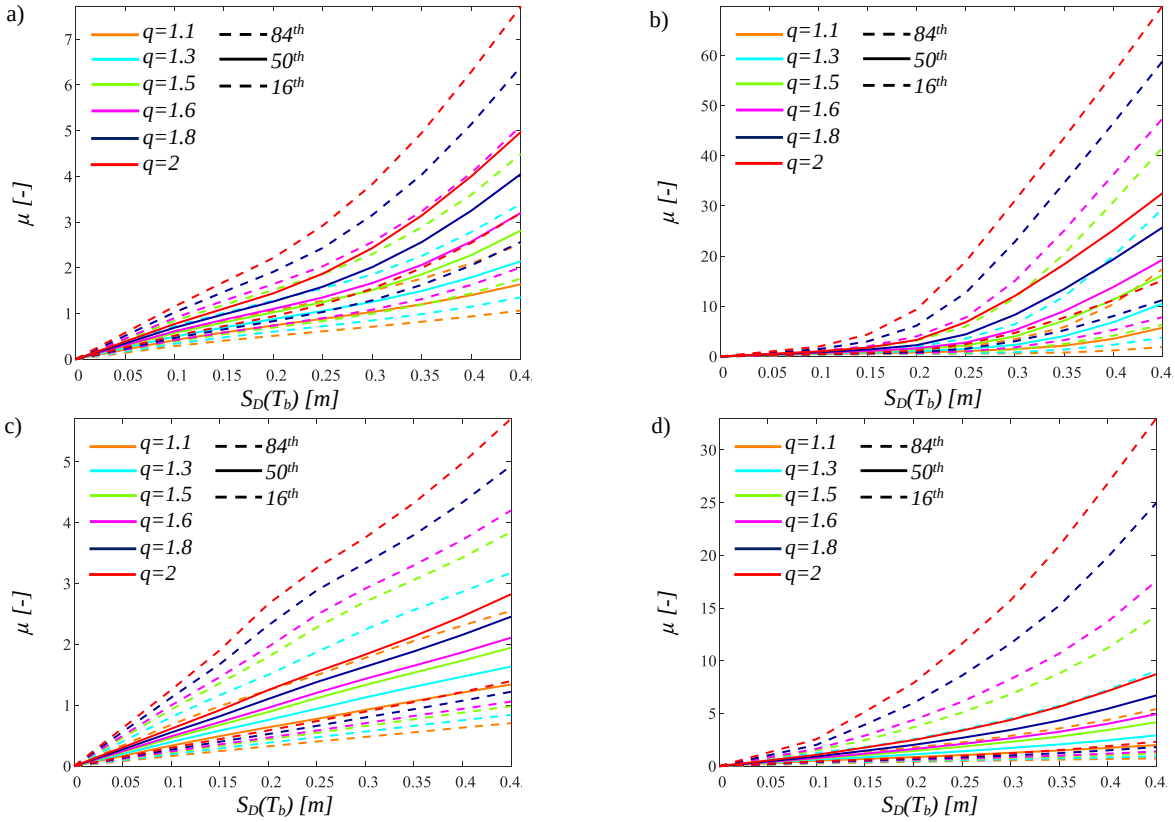

Figure 6: IDA curves of the superstructure with γ_s=0.6 for I_d=2, T_b=3 s, H=0.03 (a), I_d=2, T_b=6 s, H=0.03 (b), I_d=8, T_b=3 s, H=0.03 (c), I_d=8, T_b=6 s, H=0.03 (d).

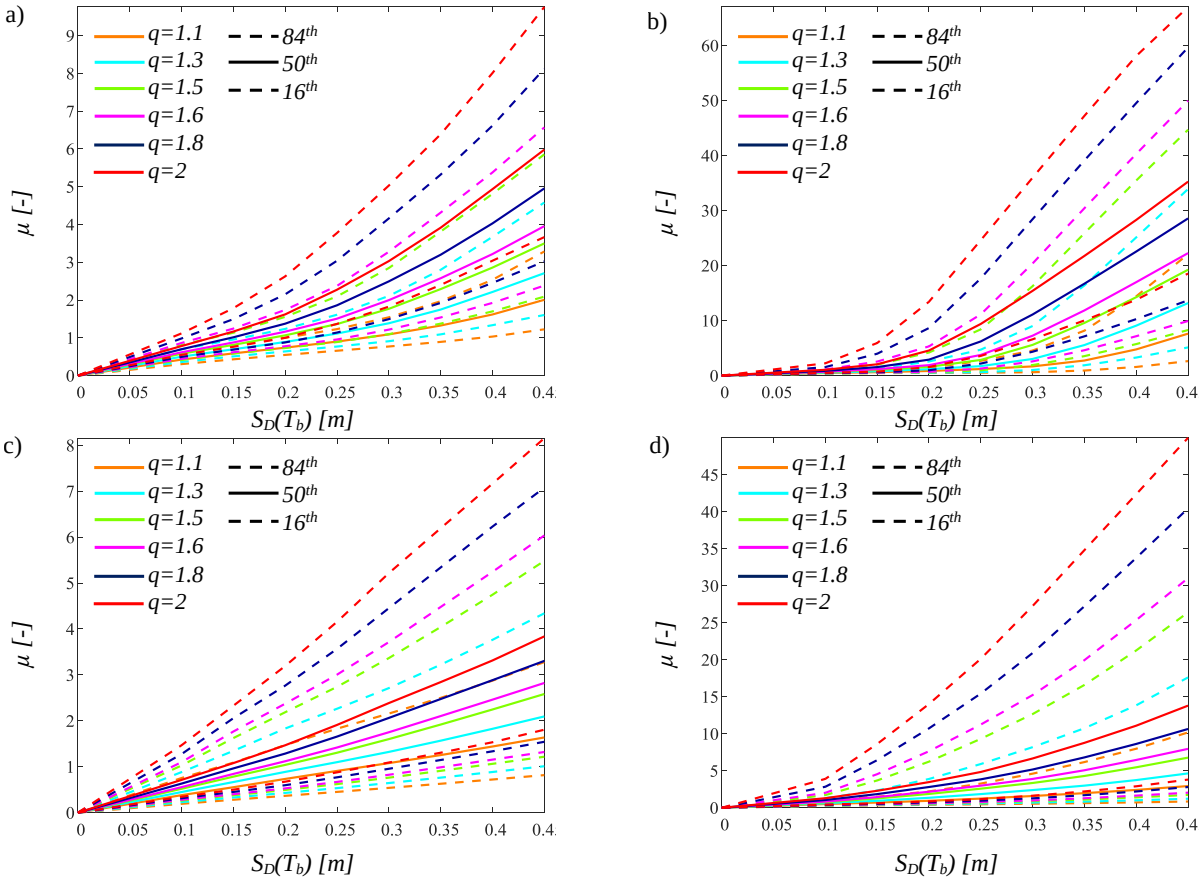

Figure 7. IDA curves of the superstructure with γ_s=0.8 for I_d=2, T_b=3 *s*, *H*=0.03 (a), I_d=2, T_b=6 s, *H*=0.03 (b), I_d=8, T_b=3 s, *H*=0.03 (c), I_d=8, T_b=6 s, *H*=0.03 (d).

5 SEISMIC FRAGILITY CURVES

Defined the limit states, respectively, in terms of the radii in plan for the two surfaces of the DFPS device, $r_1[m]$ and $r_2[m]$, and of the displacement ductility for the superstructure, μ *[-]*, the seismic fragility, representative of the probabilities P_f exceeding the different limit states at each level of the *IM*, is evaluated. Tables 1-2 report, respectively, the failure probabilities in 50 years [54],[55] with the corresponding *LS* thresholds, related to the *LS*s provided by the codes [33]-[34]: the failure probability in 50 years [18],[54],[55] corresponding to the collapse *LS* [34] for the DFPS; whereas, the failure probability in 50 years [18],[54],[55] corresponding to the life safety *LS* [34] for the superstructure in compliance with the design. The limit state thresholds of Table 1 are also used to assess the fragility in terms of the overall displacement demand to the DFPS. For the both *LS*s, several thresholds are considered with the aim to provide reliable *LS* thresholds for these systems. For each parameter combination (384 equivalent 3dof systems), the probabilities P_f exceeding the different *LS*s at each *IM* level, are numerically computed and then fitted through lognormal distributions [19] with a R-square value higher than 0.8.

	$LS_{r,1}$	$LS_{r,2}$	$LS_{r,3}$	$LS_{r,4}$	$LS_{r,5}$	$LS_{r,6}$	$LS_{r,7}$	$LS_{r,8}$	$LS_{r,9}$	$LS_{r,10}$
r_i *[m] for i =1,2*	0.05	0.1	0.15	0.2	0.25	0.3	0.35	0.4	0.45	0.5
p_f*(50 years)=1.5·10*$^{-3}$										

Table 1: Limit state thresholds for the two surfaces of the DFPS with the associated exceeding probability.

	$LS_{\mu,1}$	$LS_{\mu,2}$	$LS_{\mu,3}$	$LS_{\mu,4}$	$LS_{\mu,5}$	$LS_{\mu,6}$	$LS_{\mu,7}$	$LS_{\mu,8}$	$LS_{\mu,9}$	$LS_{\mu,10}$
μ [-]	1	2	3	4	5	6	7	8	9	10
pf (50 years)=2.2·10^{-2}										

Table 2: Limit state thresholds for the superstructure with the associated exceeding probability.

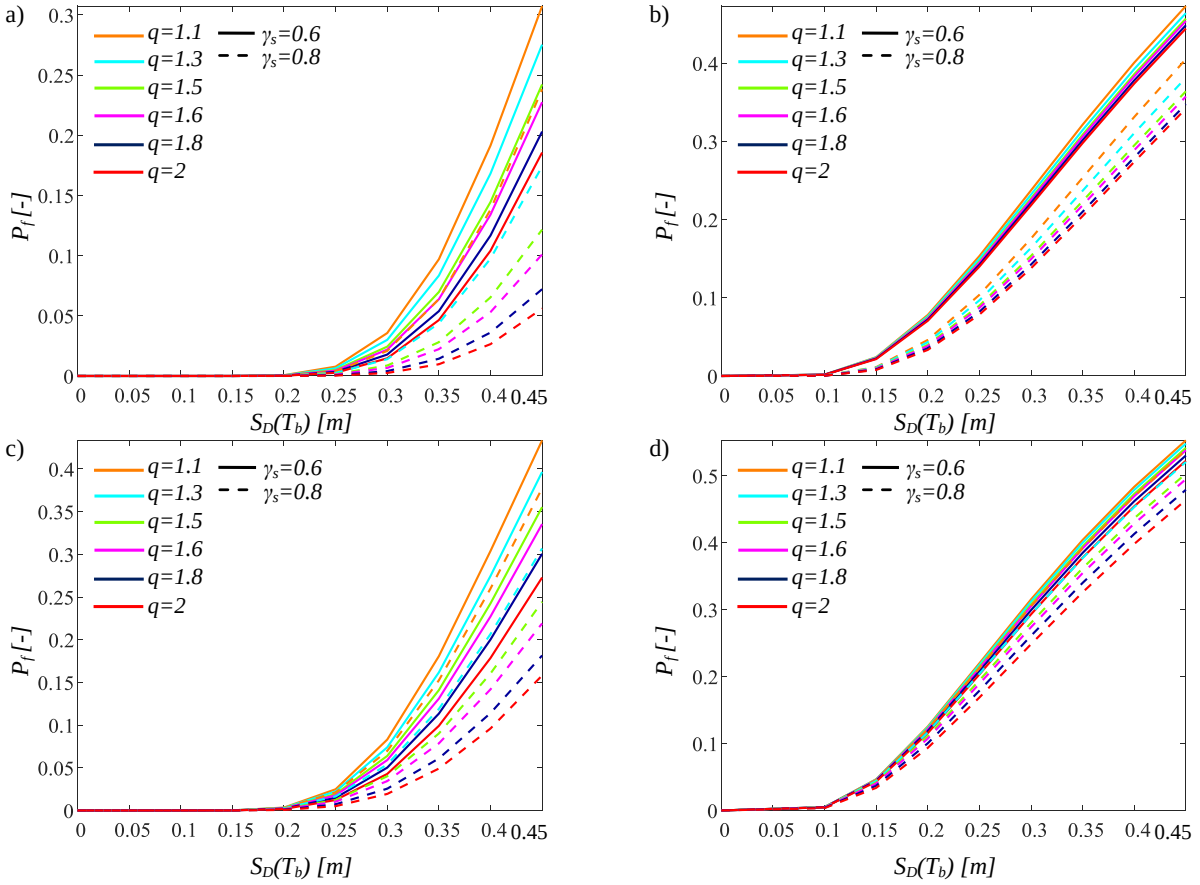

Figure 8: Seismic fragility curves of the isolation level related to $LS_{r,4}$=0.2 m, for I_d=2, T_b=3 s, H=0.03 (a), I_d=2 and T_b=6 s, H=0.03 (b), I_d=8 and T_b=3 s, H=0.03 (c), I_d=8 and T_b=6 s, H=0.03 (d).

Fig.s 8-11 depict the fragility curves (i.e., the exceeding probabilities P_f (complementary distribution functions (CCDFs))) versus the *IM* for hardening. Precisely, the curves corresponding to the different structural properties of interest and related only to some *LS* thresholds ($LS_{r,4}$ and $LS_{\mu,3}$) and to I_d =8 and T_b =3s, are represented. Generally, the seismic fragility of each degree of freedom decreases for increasing the corresponding *LS* threshold.

For the all limit states, the exceeding probabilities slightly increase for decreasing γ_s. Then, especially for high limit state thresholds, the fragility decreases by decreasing T_b, I_d and increasing q. Note that the probability exceeding a limit state is quite low for the single surface, with a lower probability for the surface 2 characterized by a lower friction coefficient with a lower radius of curvature, in compliance with the IDA results.

The fragility curves of the nonlinear hardening superstructures are shown in Fig. 11. The exceeding probabilities are slightly higher as γ_s increases but highly increase for increasing values of q.

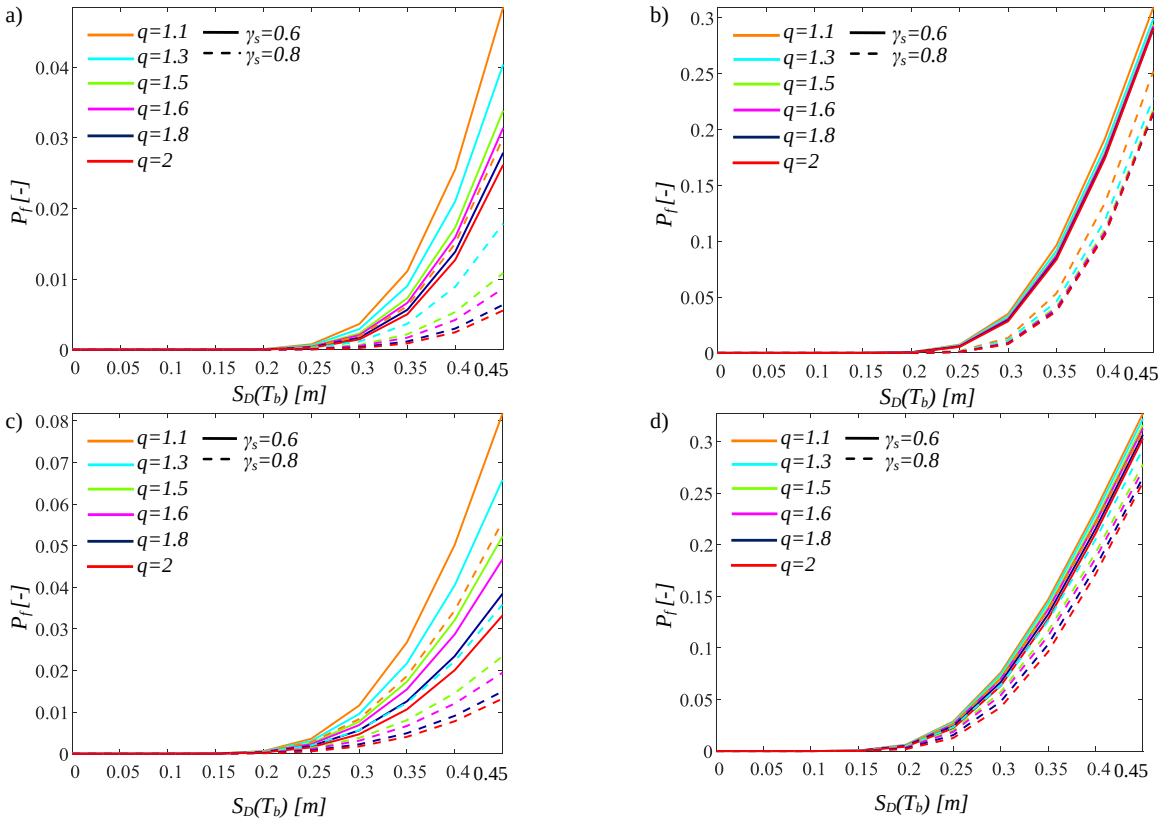

Figure 9: Seismic fragility curves of the sliding surface 1 related to $LS_{r,4}$=0.2 m, for I_d=2, T_b=3 s, H=0.03 (a), I_d=2 and T_b=6 s, H=0.03 (b), I_d=8 and T_b=3 s, H=0.03 (c), I_d=8 and T_b=6 s, H=0.03 (d).

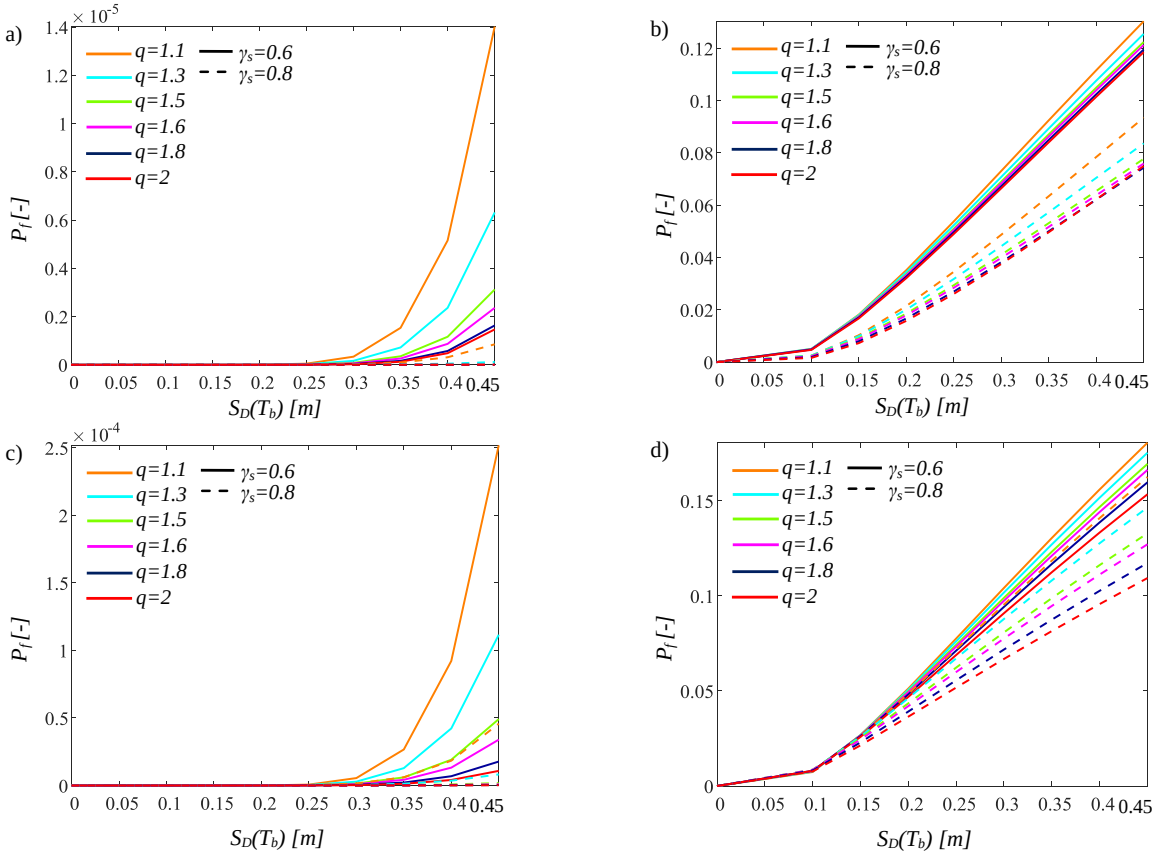

Figure 10: Seismic fragility curves of the sliding surface 2 related to $LS_{r,4}$=0.2 m, for I_d=2, T_b=3 s, H=0.03 (a), I_d=2 and T_b=6 s, H=0.03 (b), I_d=8 and T_b=3 s, H=0.03 (c), I_d=8 and T_b=6 s, H=0.03 (d).

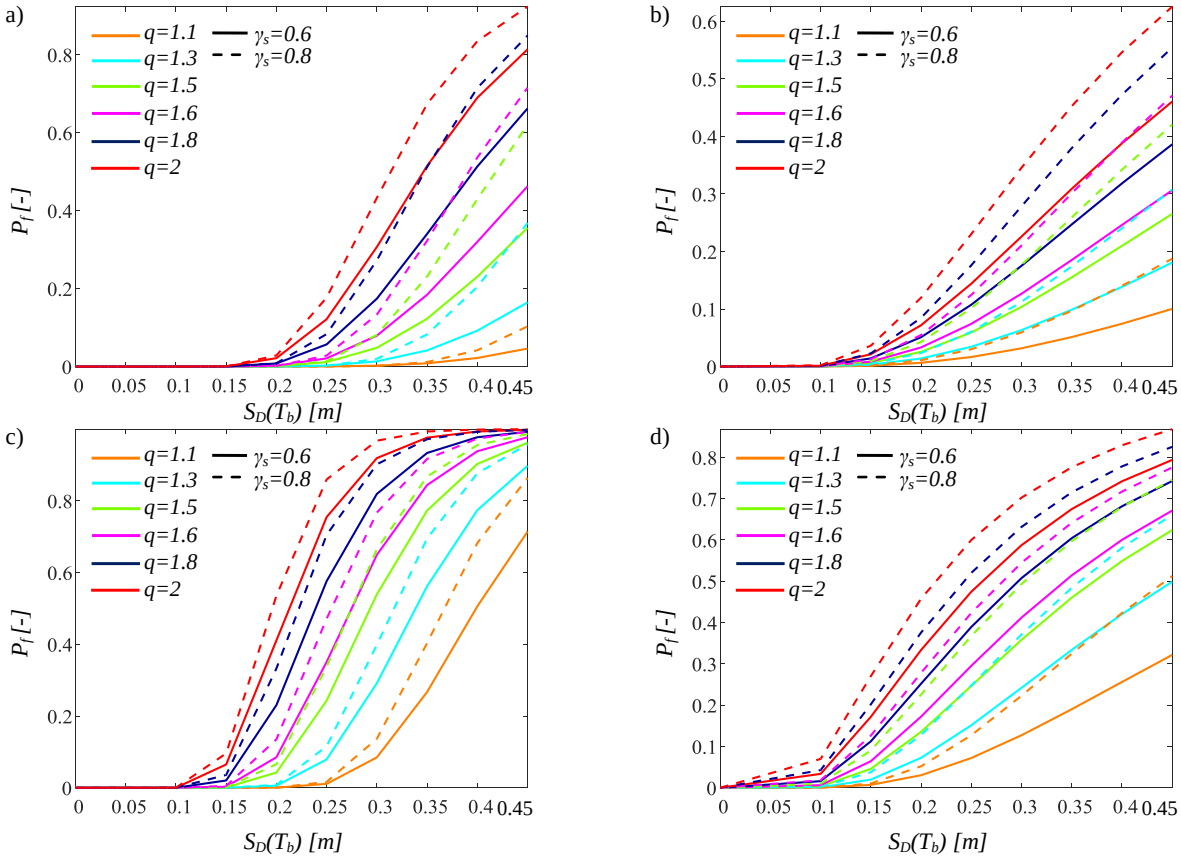

Figure 11: Seismic fragility curves of the superstructure related to $LS_{\mu,3}$=3, for I_d=2, T_b=3 s, H=0.03 (a), I_d=2 and T_b=6 s, H=0.03 (b), I_d=8 and T_b=3 s, H=0.03 (c), I_d=8 and T_b=6 s, H=0.03 (d).

Conversely, higher values of T_b for fixed I_d lead to a decrease of the seismic fragility because an increase of the period T_s means an increase of the correlated yielding displacement as well as lower values of T_b for fixed I_d lead to higher values of the seismic fragility. In fact, the coupling between I_d and T_b is a very important parameter because it defines T_s and the corresponding yielding displacement. Therefore, as also discussed in [41]-[42], in the case of systems with low T_s, the ensuing dynamic amplification can cause disproportioned superstructure responses and, so a high seismic fragility derives. These resonance effects, are reduced with respect to the outcomes of [41] in the case of the post-yield hardening stiffness ratio. Comparing the result with the outcomes of [42], the hardening systems have slightly higher probability exceeding a limit state for higher value of T_b, and the influence of γ_s is more marked.

6 SEISMIC PERFORMANCE OF INELASTIC STRUCTURES WITH DFPS

The convolution integral between the previously achieved seismic fragility curves and the seismic hazard curves expressed in terms of the same *IM*, $S_D(T_b)$, related to the reference site (L'Aquila (Italy)), allows the evaluation of the mean annual rates exceeding the limit states for each parameter combination. Then, by using a Poisson distribution, the seismic reliability of the all hardening structures isolated by DFPS in the time frame of interest (e.g., 50 years) have been computed. In this work, the seismic hazard of L'Aquila site (Italy), soil class B,

with geographic coordinates 42°38'49''N and 13°42'25''E, has been considered, as widely described in [41].

As for the DFPS devices, the seismic reliability evaluation makes it possible to define SRBD curves to design the dimensions in plan of each surface of these devices and the overall dimension of the isolation level as a function of the expected reliability level and of the structural properties.

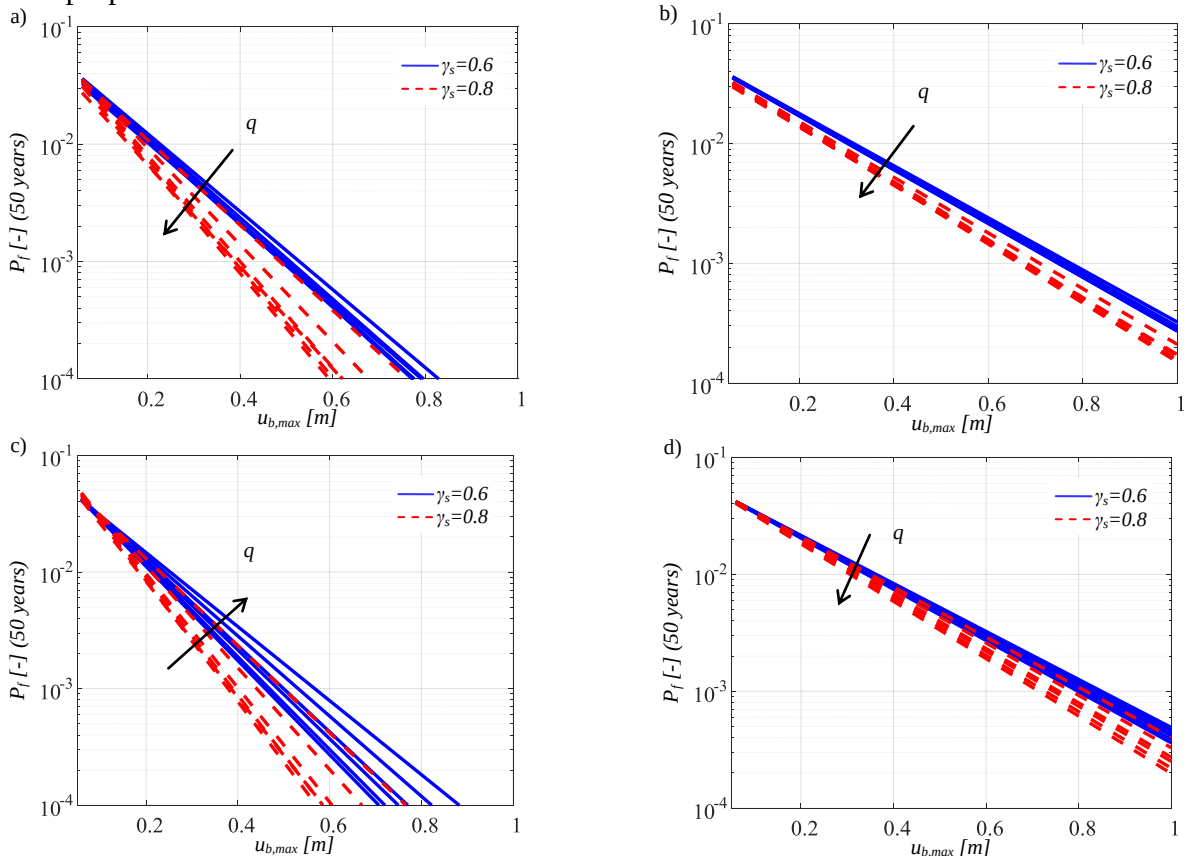

Figure 12: Seismic reliability curves of the isolation level related to I_d=2, T_b=3 s, H=0.03 (a), I_d=2 and T_b=6 s, H=0.03 (b), I_d=8 and T_b=3 s, H=0.03 (c), I_d=8 and T_b=6 s, H=0.03 (d). The arrow denotes the increasing direction of q.

Fig. 12 depicts the linear regressions representative of the seismic reliability of the overall dimension of the isolation level, in the semi-logarithmic space. The value of R-square is higher than 0.9. These curves show that an exceeding probability of $P_f = 1.5 \cdot 10^{-3}$ (corresponding to the collapse *LS*, in 50 years) [54]-[57] requires a global dimension ranging from about 0.3 m to about 1 m depending on the structural properties. The overall dimension of the isolation level estimated with the above described curves, can also be useful to define the radius in plan of each surface of the DFPS. In fact, SRBD curves of each surface, evaluated and not represented due to space constrains, highlighted that around 1/3 of the global dimension can be attributed to the surface 2 (having a lower friction coefficient with a lower radius of curvature) and 2/3 to the surface 1 for low T_b, whereas for high T_b, these ratios become 1/4 and 3/4, respectively. This aspect is a very important design feature because if high displacements are required to the isolation level are divided between the two sliding surfaces reducing the geometric encumbrance of the itself device and of the structural elements directly connected as also highlighted in [28]-[30].

Fig. 13 shows the results, representative of the SP curves of the hardening superstructure in 50 years, in the logarithmic scale for the different *LS* thresholds in terms of μ and for the dif-

ferent structural properties. The seismic reliability of the superstructure increases for low values of γ_s, I_d, q and for high values of T_b. Comparing the results with the outcomes achieved by [42], the seismic reliability of systems equipped with DFPS, with different friction coefficients for the two surfaces, is slightly lower respect the systems equipped with simple FPS due to the reasons previously explained for the fragility assessment.

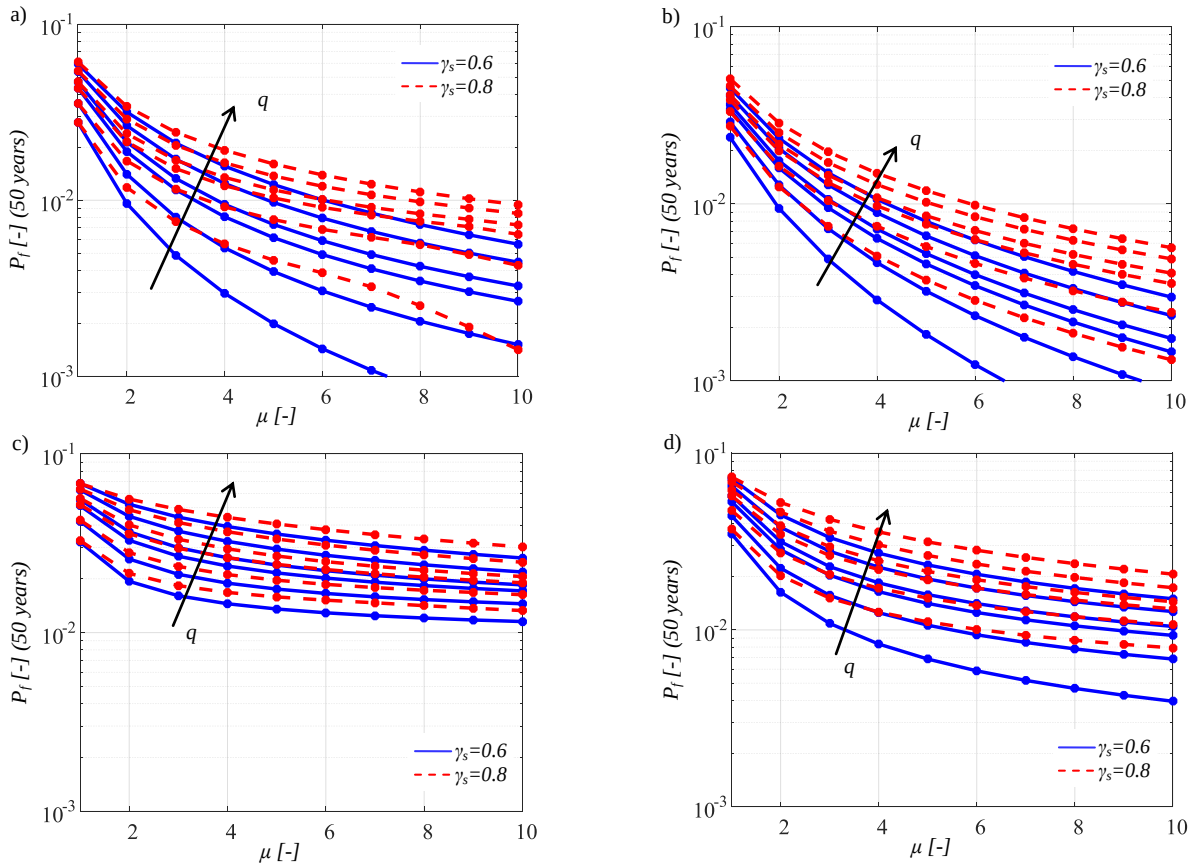

Figure 13: Seismic reliability curves of the superstructure related to I_d=2, T_b=3 s, H=0.03 (a), I_d=2 and T_b=6 s, H=0.03 (b), I_d=8 and T_b=3 s, H=0.03 (c), I_d=8 and T_b=6 s, H=0.03 (d). The arrow denotes the increasing direction of q.

7 CONCLUSIONS

This study describes the seismic reliability-based performance of hardening structural systems equipped with double concave sliding devices isolators on varying the elastic and inelastic building properties, seismic intensity levels with the hypothesis of the friction coefficients and of the characteristics of the seismic records assumed as the relevant random variables. By means of an equivalent 3dof system with a non-linear velocity-dependent model for the two surfaces of the DFPS, incremental dynamic analyses are carried out considering several natural seismic records, the seismic hazard of L'Aquila site (Italy), increasing behavior factors and different post-yield stiffness ratios. Then, the seismic fragility curves are derived for the hardening superstructure and for the isolation level taking also into account the dynamic failure cases. After that, assuming a design life of 50 years, seismic reliability-based design (SRBD) curves are proposed useful to design the radii in plan of the two surfaces as well as the maximum demand to the DFPS. The results have highlighted the negative effects of the post-yield stiffness as well as the possibility to reduce the encumbrance of the devices and of the struc-

tural elements directly connected because the seismic demand is divided on the two surfaces. This aspect is a very important design feature of the DFPS representing an its advantage.

Regarding the non-linear hardening superstructures, the seismic reliability-based linear regressions demonstrate the positive influence of the overstrength hardening properties able to reduce the displacement ductility demand. From the analysis of the seismic reliability-based results, an upper values of 1.5 for the behaviour factor is compatible with all the structural properties for hardening systems with DFPS. The proposed SRBD curves can be useful for a preliminary and reliable design or verification of regular frames, not sensitive to the $P-\Delta$ effects, equipped with DFPS and located in a high seismic hazard area.

REFERENCES

[1] Christopoulos C, Filiatrault A. *Principles of Passive Supplemental Damping and Seismic Isolation*. IUSS Press: Pavia, Italy, 2006.

[2] Zayas VA, Low SS, Mahin SA. A simple pendulum technique for achieving seismic isolation. *Earthquake Spectra* 1990; 6:317–33.

[3] Su L, Ahmadi G, Tadjbakhsh IG. Comparative study of base isolation systems. *Journal of Engineering Mechanic* 1989; 115:1976–92.

[4] Mokha A, Constantino MC, Reinhorn AM. Teflon Bearings in Base Isolation. I: *Testing. J. Struct. Eng. 1990;* 116(2): 438-454.

[5] Constantinou MC, Mokha A, Reinhorn AM. Teflon Bearings in Base Isolation. II: *Modeling. J. Struct. Eng.* 1990; 116(2):455-474.

[6] Constantinou MC, Whittaker AS, Kalpakidis Y, Fenz DM, Warn GP. *Performance of Seismic Isolation Hardware Under Service and Seismic Loading. Technical Report*, 2007.

[7] Almazàn JL, De la Llera JC. Physical model for dynamic analysis of structures with FPS isolators. Earthquake Engineering and Structural Dynamics 2003; 32:1157–1184.

[8] Ayyub BM, McCuen RH. *Probability, statistics, and reliability for engineers. 2nd ed.* NY: CRC Press; 2002.

[9] Lin YK, Cai GQ. *Probabilistic structural dynamics—advanced theory and applications*. NY: McGraw-Hill; 1995.

[10] Chen J, Liu W, Peng Y, Li J. Stochastic seismic response and reliability analysis of base-isolated structures. *J Earthquake* Eng 2007;11:903–24.

[11] Alhan C, Gavin HP. Reliability of base isolation for the protection of critical equipment from earthquake hazards. *Eng Struct* 2005;27:1435–49.

[12] Han R., Li Y., van de Lindt J., Seismic risk of base isolated non-ductile reinforced concrete buildings considering uncertainties and mainshock–aftershock sequences, *Structural Safety,* 50, 39-56, 2014.

[13] Zou XK, Wang Q, Li G, Chan CM. Integrated reliability-based seismic drift design optimization of base-isolated concrete buildings. *J Struct Eng* 2010;136:1282–95.

[14] Mishra SK, Roy BK, Chakraborty S. Reliability-based-design-optimization of base isolated buildings considering stochastic system parameters subjected to random earthquakes. *Int J Mech Sci* 2013;75:123–33.

[15] Castaldo, P, Tubaldi, E. Influence of FPS bearing properties on the seismic performance of base-isolated structures. *Earthquake Engineering and Struct. Dynamics*, 44;15: 2817–2836, 2015.

[16] Castaldo P, Palazzo B, Della Vecchia P. Seismic reliability of base-isolated structures with friction pendulum bearings. *Engineering Structures* 2015;95:80-93.

[17] Palazzo B, Castaldo P, Della Vecchia P. Seismic reliability analysis of base-isolated structures with friction pendulum system, *2014 IEEE Workshop on Environmental, Energy and Structural Monitoring Systems Proceedings*, Napoli, September 17-18, 2014.

[18] Castaldo P., Palazzo B., Della Vecchia P., "Life-cycle cost and seismic reliability analysis of 3D systems equipped with FPS for different isolation degrees*", Engineering Structures*, 125;349–363, http://dx.doi.org/10.1016/j.engstruct.2016.06.056, 2016.

[19] Castaldo P., Amendola G., Palazzo B.,"Seismic fragility and reliability of structures isolated by friction pendulum devices: Seismic reliability-based design (SRBD)", *Earthquake Engineering and Structural Dynamics*, 46(3); 425–446, DOI: 10.1002/eqe.2798, 2017.

[20] Castaldo P, Mancini G, Palazzo B., Seismic reliability-based robustness assessment of three-dimensional reinforced concrete systems equipped with single-concave sliding devices. *Engineering Structures* 163:373-387, 2018

[21] Castaldo P., Ripani M., "Optimal design of friction pendulum system properties for isolated structures considering different soil conditions", *Soil Dynamics and Earthquake Engineering*, 2016, 90:74–87, DOI: 10.1016/j.soildyn.2016.08.025.

[22] Castaldo, P., Tubaldi, E., Influence of ground motion characteristics on the optimal single concave sliding bearing properties for base-isolated structures. *Soil Dynamics and Earthquake Engineering*, 104: 346–364, 2018.

[23] Roy B.K., Chakraborty S., Robust optimum design of base isolation system in seismic vibration control of structures under random system parameters, *Str. Safety*, 55: 49-59, 2015.

[24] Bucher C. Probability-based optimal design of friction-based seismic isolation devices, *Structural Safety*, 31(6): 500-507, 2009.

[25] Castaldo, P., Lo Priore, R. Seismic performance assessment of isolated bridges for different limit states, *J Civil Struct Health Monit* 8(1): 17–32, 2018.

[26] Kim Y.S., Yun C.B. Seismic response characteristics of bridges using double concave friction pendulum bearings with tri-linear behavior. *Engin. Struct. 29* (2007) 3082-3093, 2007.

[27] Castaldo P, Ripani M, Lo Piore R Influence of soil conditions on the optimal sliding friction coefficient for isolated bridges. *Soil Dynamics and Earthquake Engineering* 111:131–148, https://doi.org/10.1016/j.soildyn.2018.04.056, 2018.

[28] Fenz D.M, Constantinou M.C., Behaviour of the double concave friction pendulum bearing. *Earthquake Engineering and Structural Dynamics*, 2006; 35:1403-1424, 2006.

[29] Constantinou M.C., *Friction pendulum double concave bearings, technical report.* University of Buffalo NY, October 29, 2004.

[30] Tsai C.S., Chiang T.C., Chen B.J., Experimental evaluation of piecewise exact solution for predicting seismic responses of spherical sliding type isolated structures. *Earthquake Engineeering and Structural Dynamics* 2005;34:1027-1046 DOI: 10.1002/equ.430.

[31] Soni D.P., Mistry B.B., Panchal V.R., Double variable frequency pendulum isolator for seismic isolation of liquid storage tanks. *Nuclear Engineering and Design*, Volume 241, issue 3, march 2011:700-713.

[32] Structural Engineering Institute. Minimum design loads for buildings and other structures (Vol. 7, No. 5). *Amer Society of Civil Engineers*, 2010.

[33] European Committee for Standardization. *Eurocode 8-Design of Structures for Earthquake Resistance. Part 1: General Rules, Seismic Actions and Rules for Buildings,* Brussels, 2004.

[34] NTC18. *Norme tecniche per le costruzioni.* Gazzetta Ufficiale del 20.02.18, DM 17.01.18, Ministero delle Infrastrutture.

[35] Japanese Ministry of Land, Infrastructure and Transport, *Notification No. 2009–2000, Tech. Standard for Structural Specif.s and Calculation of Seismically Isolated Buildings* 2000.

[36] *Quantification of Building Seismic Performance Factors, FEMA P695* / June 2009.

[37] Occhiuzzi, A, Veneziano, D.and Van Dyck, J. (1994) *Seismic design of base isolated structures*, Savidis (Ed.), Balkema, Rotterdam, NL.

[38] Vassiliou M.F., Tsiavos A., Stojadinović B. Dynamics of inelastic base-isolated structures subjected to analytical pulse ground motions. *Eart. Eng. and Str. Dyn.* 2013; 42:2043–2060.

[39] Newmark NM, Hall WJ. *Seismic design criteria for nuclear reactor facilities, Report 46, Building Practices for Disaster Mitigation*, National Bureau of Standards, 1973.

[40] Miranda E, Bertero VV. Evaluation of strength reduction factors for earthquake-resistant design. *Earthquake Spectra* 1994; 10:357–379.

[41] Castaldo P., Palazzo B., Ferrentino T., "Seismic reliability-based ductility demand evaluation for inelastic base-isolated structures with friction pendulum devices", *Earthquake Engineering and Structural Dynamics*, 46(8): 1245-1266, DOI: 10.1002/eqe.2854, 2017.

[42] Castaldo P., Palazzo B., Alfano G., Palumbo M.F., "Seismic reliability-based ductility demand for hardening and softening structures isolated by friction pendulum bearings", *Structural Control and Health Monitoring*, 25(11),e2256, 2018.

[43] Mckey MD, Conover WJ, Beckman RJ. A comparison of three methods for selecting values of input variables in the analysis from a computer code. *Technometrics* 1979;21:239-45.

[44] Vořechovský M, Novák D. Correlation control in small-sample Monte Carlo type simulations I: a simulated annealing approach. *Probabilistic Engineering Mechanics* ;24(3):452–62, 2009.

[45] Celarec D, Dolšek M. The impact of modelling uncertainties on the seismic performance assessment of reinforced concrete frame buildings. *Engineering Structures*;52:340–354, 2013.

[46] Hong H-K, Liu C-S Internal symmetry in bilinear elastoplasticity, *International Journal of Non-Linear Mechanics*, 34:279–288, 1999.

[47] Hatzigeorgiou GD. Ductility demand spectra for multiple near- and far-fault earthquakes. *Soil Dynamics and Earthquake Engineering*;30 170-183, 2010.

[48] Hatzigeorgiou GD, Papagiannopoulos GA, Beskos DE. Evaluation of maximum seismic displacements of SDOF systems form their residual deformation. *Engineering Structures 2011;33 3422-3431.*

[49] Naeim F, Kelly JM. *Design of Seismic Isolated Structures: From Theory to Practice.* John Wiley & Sons, Inc.; 1999.

[50] Gupta A, Krawinkler H. Seismic demands for performance evaluation of steel moment resisting frame structures. *The John A. Blume Earth. Eng. Center report No. 132*, June 1999.

[51] Adam C, Ibarra LF, Krawinkler H. Evaluation of P-Delta effects in non-deteriorating MDOF structures from equivalent SDOF systems. *13th Word Conference on Earthquake Engineering, Vancouver, B.C., Canada* 2004, Paper No. 3407, 2004.

[52] Palazzo B. Seismic Behavior of base-isolated Buildings. *Proc. International Meeting on earthquake Protection of Buildings, Ancona*, 1991.

[53] Collins KR, Stojadinovic B. Limit states for performance-based design. *12WCEE*, 2000.

[54] Bertero RD, Bertero VV. Performance-based seismic engineering: the need for a reliable conceptual comprehensive approach. *Earthquake Engineering and Structural Dynamics 2002*;31:627–652 (DOI: 10.1002/eqe.146), 2002.

[55] Aoki Y, Ohashi Y, Fujitani H, Saito T, Kanda J, Emoto T, Kohno M. Target seismic performance levels in structural design for buildings. *12WCEE*, 2000.

[56] SEAOC Vision 2000 Committee. *Performance-based seismic engineering. Report prepared by Structural Engineers Association of California,* Sacramento, CA., 1995.

[57] CEN – *European Committee for Standardization. Eurocode 0: Basis of Structural Design. Final draft*. Brussels, 2006.

[58] Saito T, Kanda J, Kani N. Seismic reliability estimate of building structures designed according to the current Japanese design code. *Proc.s of the Str. Eng.s World Congress*, 1998.

[59] Cornell CA, Krawinkler H. *Progress and challenges in seismic performance assessment*. PEER Center News 2000;4(1):1-3

[60] Aslani H, Miranda E. Probability-based seismic response analysis. *Engineering Structures 2005*; 27(8): 1151-1163, 2005.

[61] Porter KA. An overview of PEER's performance-based earthquake engineering methodology. *Proceedings, Proceedings of the 9th International Conference on Application of Statistics and Probability in Civil Engineering (ICASP9)*, San Francisco, California, 2003; 973-980.

[62] Kulkarni JA, Jangid RS. Effects of superstructure flexibility on the response of base-isolated structures. *Shock and Vibration* 2003;26:1-13, 2003.

[63] http://www.fipindustriale.it/

[64] Shome N, Cornell CA, Bazzurro P, Carballo JE. Earthquake, records, and nonlinear responses. *Earthquake Spectra*; 14(3): 469-500, 1998.

[65] Luco N, Cornell CA. Structure-specific scalar intensity measures for near-source and ordinary earthquake ground motions. *Earthquake Spectra*; 23(2): 357-92, 2007.

[66] Pinto PE, Giannini R, Franchin P. *Seismic Reliability Analysis of Structures*, IUSS Press, Pavia, Italy, 2003.

[67] Ryan KL, Chopra AK., Estimation of Seismic Demands on Isolators Based on Nonlinear Analysis. *J. Struct. Eng.*, 130(3), 392–402, 2004.

[68] PEER, Pacific Earthquake Engineering Research Center http://peer.berkeley.edu/

[69] ITACA, Italian Accelerometric Archive http://itaca.mi.ingv.it/ItacaNet/itaca10_links.htm

[70] ISESD, Internet-Site for European Strong-Motion Data http://www.isesd.hi.is/ESD_Local/frameset.htm

[71] Vamvatsikos D, Cornell CA. Incremental dynamic analysis. Earthquake *Engineering and Structural Dynamics 2002*; 31(3): 491–514, 2002.

[72] Math Works Inc. MATLAB-High Performance Numeric Computation and Visualization Software. User's Guide. Natick: MA, USA, 1997.

[73] Castaldo P, Gino D, Carbone VI, Mancini G. Framework for definition of design formulations from empirical and semi-empirical resistance models, Structural Concrete, 19(4), 980-987, 2018 https://doi.org/10.1002/suco.201800083.

[74] Castaldo, P., De Iuliis, M. (2014) Effects of deep excavation on seismic vulnerability of existing reinforced concrete framed structures, Soil Dynamics and Earthquake Engineering 64, 102-112.

[75] Castaldo, P., Palazzo, B., Perri, F. (2016) Fem simulations of a new hysteretic damper: The dissipative column, Ingegneria Sismica, 33(1), 34-45.

[76] Castaldo, P., Calvello, M., Palazzo, B. (2013) Probabilistic analysis of excavation-induced damages to existing structures, Computers and Geotechnics, 53, 17-30.

[77] Castaldo P, Gino D, Bertagnoli G, Mancini G. Partial safety factor for resistance model uncertainties in 2D non-linear finite element analysis of reinforced concrete structures, Engineering Structures, 176(2018), 746-762.

[78] Castaldo, P., Jalayer, F., Palazzo, B. (2018) Probabilistic assessment of groundwater leakage in diaphragm wall joints for deep excavations, Tunnelling and Underground Space Technology 71, 531-543.

[79] Zanini M.A., Faleschini F., Zampieri P., Pellegrino C., Gecchele G., Gastaldi M., Rossi R. (2017) Post-quake urban road network functionality assessment for seismic emergency management in historical centers. Structure and Infrastructure Engineering, 13(9): 1117-1129

[80] Zanini M.A., Faleschini F., Pellegrino C. (2017) Probabilistic seismic risk forecasting of aging bridge networks. Engineering Structures, 136: 219-232

[81] Zanini M.A., Hofer L., Faleschini F., Zampieri P., Fabris N., Pellegrino C. (2016) Preliminary macroseismic survey of the 2016 Amatrice seismic sequence. Annals of Geophysics, 59(5), 6. ISSN: 1593-5213, DOI: 10.4401/ag-7172

[82] Faleschini F., Bragolusi P., Zanini M.A., Zampieri P., Pellegrino C. (2017) Experimental and numerical investigation on the cyclic behavior of RC beam-column joints with EAF slag concrete. Engineering Structures, 152: 335-347

[83] Faleschini F., Gonzalez-Libreros J., Zanini M.A., Hofer L., Sneed L.H., Pellegrino C. (2019) Repair of severely damaged RC exterior beam-column joints with FRP and FRCM composites. Composite Structures, 207: 352-363

[84] Cavaleri L, Di Trapani F, Macaluso G, Papia M (2012) Reliability of code proposed models for assessment of masonry elastic moduli. Ing Sismica 29(1):38–59.

[85] Campione, G., Cavaleri, L., Di Trapani, F. and Ferrotto, M.F. (2017), "Frictional effects on structural behavior of no-endconnected steel-jacketed RC columns: Experimental results and new approaches to model numerical and analytical response", J. Struct. Eng., ASCE, 143(8), 04017070.

[86] Campione G, Cavaleri L, Di Trapani F, Macaluso G, Scaduto G (2016) Biaxial deformation and ductility domains for engineered rectangular RC cross-sections: a parametric study highlighting the positive roles of axial load, geometry and materials. Eng Struct 107(15):116–134

[87] Di Trapani, F., Bertagnoli, G., Ferrotto, M.F., Gino, D. Empirical equations for the direct definition of stress-strain laws for fiber-section-based macromodeling of infilled frames 2018. Journal of Engineering Mechanics 144(11),04018101.

[88] Cavaleri L, Di Trapani F, Asteris PG, Sarhosis V (2017) Infuence of column shear failure on pushover based assessment of masonry inflled reinforced concrete framed structures: a case study. Soil Dyn Earthq Eng 100:98–112.

[89] Seismic fragility assessment of infilled frames subject to mainshock/aftershock sequences using a double incremental dynamic analysis approach Di Trapani, F., Malavisi, M. 2019 Bulletin of Earthquake Engineering 17(1), pp. 211-235.